Far-field superresolution by imaging of resonance scattering

Gerard T. Schuster and Yunsong Huang*
King Abdullah University of Science and Technology

SUMMARY

We show that superresolution imaging in the far-field region of the sources and receivers is theoretically possible if migration of resonant multiples is employed. A resonant multiple is one that bounces back and forth between two scattering points or two neighboring reflectors. For a source with frequency f, N roundtrips in propagating between two scatterers increases the effective frequency to $2N \times f$ and decreases the effective wavelength λ to $\lambda/2N$. Thus, interbed multiples can, in principle, be used as high-frequency probes to estimate detailed properties of layers. This is not only applicable to crustal reflections, but also to mantle and core reverberations of interest to earthquake seismologists.

INTRODUCTION

The resolution limit is important for defining the minimum distance Δx between two neighboring objects in which they are distinguishable in the migration image. Superresolution imaging that beats the Abbe limit $\Delta x \simeq \lambda/2$ is possible if the wave energy scattered from sub-wavelength objects in the near-field of the source are refocused by TRMs to the source location (Lerosey et al., 2007; Fink, 2008). This is similar to optical imaging devices that include a super lens in the near field of the source (i.e., within a half-wavelength distance) that converts the evanescent energy to propagating waves (de Fornel, 2001). Analogous to the scanning tunneling microscope, Schuster et al. (2012) proposed a seismic scanning tunneling macroscope that harnesses the sub-wavelength imaging potential in near-field seismic energy. In this case, the evanescent energy in the near-field region is characterized by the strongly varying inverse distance term $1/r$ in the Green's functions. Such variations in the TRM profile can indicate the presence and the sub-wavelength size of nearby scatterers.

The question naturally arises: can one achieve superresolution where $\Delta x \ll \lambda/2$ in the far field of both sources and receivers? As we show in this extended abstract, the answer is yes if resonant scattered arrivals are properly migrated. As a simple example, Figure 1 depicts single- and triple-bounce scattering between two scatterers for a single source-receiver pair on the surface. Migration of the scattered event requires that the energy arriving between τ_A and τ_B in the trace should be smeared between the inner and outer portions of the Cartesian oval[1]. The triple-bounce oval is three times skinnier than the single-bounce one because the rays must traverse the b) oval band three times (see zoom view of three rays in far right of Figure 1b) to account for the time difference $\tau_B - \tau_A$; this compares to the single-bounce case a) where only one traverse is required. If the time to propagate one wavelength is one period $\approx \tau_B - \tau_A$ of time, then the Cartesian oval band in b) is about $1/3$ of a wavelength thick compared to the one-wavelength thick band in a). Skinnier migration bands lead to better resolution in the migration image.

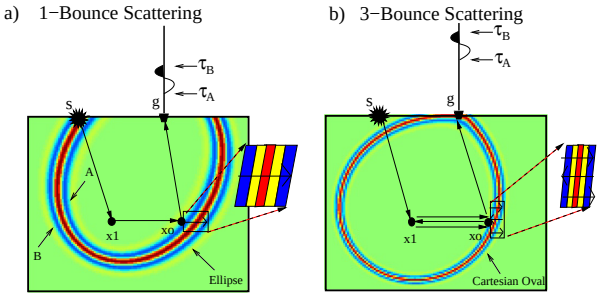

Figure 1: Migration responses of a single trace for a) single- and b) triple-bounce scattering between the scatterers at $\mathbf{x}_0$ and $\mathbf{x}_1$. The innermost part of the oval is the locus of points where $\mathbf{x}_o$ can be located and still provide the total traveltime equal to τ_A; and the outermost one is associated with the traveltime τ_B. The triple-bounce oval in b) is skinniest because there are three ray segments between the innermost and outermost ovals compared to just one in a). The total traveltime $\tau_b - \tau_a$ along the three segments must be equal to that along the single segment in a).

For a source with frequency f, N roundtrips in propagating between two scatterers decreases the effective wavelength to $\lambda/2N$. This decreased wavelength can be used to achieve superresolution imaging that is an improvement over the $\lambda/2$ diffraction limit. However, N cannot be too large because each roundtrip returns a weaker signal due to attenuation, geometrical spreading and transmission loss effects.

This abstract is organized as follows. The first part is the introduction just presented. This is followed by the theory section that presents the formalism for superresolution imaging with resonant multiples using the simple example of two scatterers. A resonant multiple is defined as the reverberation between two scatterers (or reflectors) such that the inter-scatterer rays for the multiples coincide with one another. As an example, Figure 2c depicts the triplet of parallel rays associated with resonant scattering between two scatterers. This differs from the usual multiple reflections where the raypaths for a fixed source-receiver pair do not coincide for different orders of multiples. The theoretical predictions are supported by a numerical example, and the final section presents the conclusions.

[1] A Cartesian oval is the figure consisting of all those points for which the sum of the distance to one focus ($\mathbf{x}_g$ in Figure 1) plus twice (or Nth) the distance to a second focus (i.e., $\mathbf{x}_1$ in Figure 1) is a constant. In terms of traveltimes, the Cartesian oval for a two-point scatterer in Figure 1b is the locus of points $\mathbf{x}_o$ that satisfy $\tau_{sx_1} + 3\tau_{x_1 x_o} + \tau_{x_o g} =$ constant.

DOI http://dx.doi.org/10.1190/segam2014-0344.1

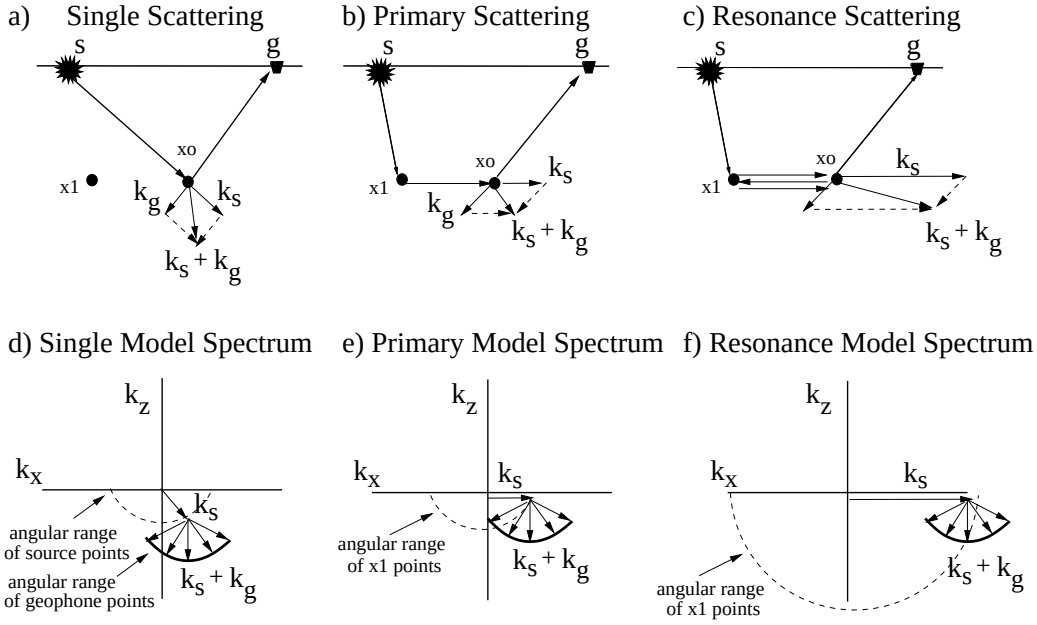

Figure 2: Ray diagrams for a) single scattering, b) primary multiple scattering and c) first-order $N = 1$ resonant scattering between the two scatterers (black filled circles). The geophone and source wavenumber vectors are denoted as $\mathbf{k}_g$ and $\mathbf{k}_s$, respectively, and each scatterer is a sub-wavelength sized reflectivity distribution centered about either $\mathbf{x}_o$ or $\mathbf{x}_1$. The reflectivity model vector estimated by migration is given by $\mathbf{k}_s + \mathbf{k}_g$; for a wide range of geophone positions the reconstructed model spectra are denoted by the thick quarter circles below each ray diagram in a)-c). The dashed semi-circles denote the model spectra associated with a wide range of source positions in d) or $\mathbf{x}_1$ scatterer positions in e) and f).

THEORY

With a simple two-scatterer example where the point scatterers can be located more than a wavelength apart from one another, we show that superresolution imaging in the far-field region of sources and receivers is possible if resonant multiples in the data are properly migrated.

Assume the two-scatterer model in Figures 2b-c where the Nth-order resonant scattering data are approximated by

$$\mathbf{g},\mathbf{s} \in B \qquad \overbrace{d(\mathbf{g}|\mathbf{s})_N}^{\mathbf{d}} = \overbrace{r_o^{2N+2} G(\mathbf{x}_1|\mathbf{s}) \int_{\Omega_{x_o}} d\mathbf{y} G(\mathbf{g}|\mathbf{y}) G(\mathbf{y}|\mathbf{x}_1)^{2N+1}}^{\mathbf{L}} \overbrace{\delta m(\mathbf{y})}^{\mathbf{m}}, \qquad (1)$$

where a localized[2] reflectivity distribution $\delta m(\mathbf{y})$ is centered at $\mathbf{y} = \mathbf{x}_o$ about the small area Ω_{x_o}, and the two neighboring scatterers each have a scattering coefficient denoted by r_o. The above equation is more compactly represented by $\mathbf{d} = \mathbf{L}\mathbf{m}$, where $\mathbf{L}$ is the forward modeling operator, $\mathbf{d}$ represents the data vector, and $\mathbf{m}$ denotes the perturbed reflectivity distribution. The line of coincident sources and receivers is directly above the two scatterers, so the integration is only over the vertical cross-section that contains both the scatterers and recording line. The point scatterer at $\mathbf{x}_1$ is assumed to be known, and the goal is to use migration of the inter-scatterer multiples to locate the scatterer's location and shape at $\mathbf{x}_o$.

The asymptotic Green's function is given by

$$G(\mathbf{x}|\mathbf{x}') = A_{xx'} e^{i\omega\tau_{xx'}}, \qquad (2)$$

for a harmonic point source at $\mathbf{x}'$, a receiver at $\mathbf{x}$, $A_{xx'}$ accounts for geometrical spreading, and ω is the angular frequency. The two scatterers are assumed to be in the far-field region of the recording line and the background medium is sufficiently smooth relative to the wavelength for the validity of the asymptotic Green's function (Bleistein, 1984). Figure 2c depicts the rays corresponding to the resonant scattering for $N = 1$ and the raypath trajectory $\mathbf{s} \to \mathbf{x}_1 \to \mathbf{x}_o \to \mathbf{x}_1 \to \mathbf{x}_o \to \mathbf{g}$, where we conveniently ignore other triple-bounce resonance such as the trajectory $\mathbf{s} \to \mathbf{x}_o \to \mathbf{x}_1 \to \mathbf{x}_o \to \mathbf{x}_1 \to \mathbf{g}$.

The Nth-order scattered data can be migrated with the Nth-order preconditioned migration kernel $\mathscr{G}(\mathbf{g},\mathbf{x},\mathbf{s})_N$:

$$\mathbf{g},\mathbf{s} \in B; \mathbf{x} \in \Omega$$
$$\mathscr{G}(\mathbf{g},\mathbf{x},\mathbf{s})^*_N = \alpha G(\mathbf{g}|\mathbf{x})^* [G(\mathbf{x}|\mathbf{x}_1)^{2N+1}]^* G(\mathbf{x}_1|\mathbf{s})^*, \qquad (3)$$

where $\mathbf{x}$ is the trial image point for the scatterer at $\mathbf{x}_o$ and $\alpha = r_o^{-2(N+1)} [A_{gx} A_{xx_1}^{2N+1} A_{x_1 s}]^{-2}$ is a convenient preconditioner to mitigate the effects of reflectance scaling and geometrical spreading in the data and migration kernel. We shall denote $\mathscr{G}(\mathbf{g},\mathbf{x},\mathbf{s})^*_N$ as a natural migration kernel because it naturally takes into account the Nth-order multiple scattering for two scatterers, one at $\mathbf{x}_1$ and the other at the trial image point $\mathbf{x}$.

[2]For convenience, we assume a sub-wavelength-sized reflectivity distribution. We will also denote this localized scatterer as a point scatterer.

DOI http://dx.doi.org/10.1190/segam2014-0344.1

Multiplying the migration kernel in equation 3 by the data in equation 1 and integrating over sources and receivers $\mathbf{g},\mathbf{s} \in B$ gives the migration image $\delta m(\mathbf{x})^{\text{mig}}$ at the trial image point $\mathbf{x} \in \Omega$:

$$\delta m(\mathbf{x})^{\text{mig}} = \overbrace{\iint_{B\times B} \mathrm{d}x_g\,\mathrm{d}x_s \mathscr{G}(\mathbf{g},\mathbf{x},\mathbf{s})^*_N}^{\mathbf{L}^T} \overbrace{d(\mathbf{g}|\mathbf{s})_N}^{\mathbf{d}}$$

$$= \overbrace{\gamma \int_B \mathrm{d}x_g \frac{G(\mathbf{g}|\mathbf{x})^* [G(\mathbf{x}|\mathbf{x}_1)^{2N+1}]^*}{[A_{gx} A^{2N+1}_{xx_1}]^2}}^{\mathbf{L}^T}$$

$$\overbrace{\int_\Omega \mathrm{d}\mathbf{y} G(\mathbf{g}|\mathbf{y}) G(\mathbf{y}|\mathbf{x}_1)^{2N+1}}^{\mathbf{L}} \overbrace{\delta m(\mathbf{y})}^{\mathbf{m}}, \qquad (4)$$

where

$$\gamma \stackrel{\text{def}}{=} \int_B \mathrm{d}x_s = |B|. \qquad (5)$$

Inserting the asymptotic Green's function in equation 2 into equation 4, restricting $\mathbf{x}$ to be near the scatterer at $\mathbf{x}_o$ and $|\mathbf{x}_o - \mathbf{g}| \gg \lambda$ gives

$$\delta m(\mathbf{x})^{\text{mig}} \approx \gamma \iint_{B\times\Omega_{\mathbf{x}_o}} \mathrm{d}x_g\,\mathrm{d}\mathbf{y} e^{i\{\overbrace{\omega(2N+1)\nabla\tau_{x_o x_1}}^{\mathbf{k}_{x_1 x_o}} + \overbrace{\omega\nabla\tau_{g x_o}}^{\mathbf{k}_{x_o g}}\}\cdot[\mathbf{y}-\mathbf{x}]}$$
$$\times \quad \delta m(\mathbf{y}) \qquad (6)$$

$$= \gamma \iint_{B\times B_{x_1'}} \mathrm{d}x_g\,\mathrm{d}x_1' \delta(x_1' - x_1) e^{-i\overbrace{\{\mathbf{k}_{x_1' x_o} + \mathbf{k}_{g x_o}\}}^{\mathbf{k}}\cdot\mathbf{x}}$$
$$\times \quad \delta M(\overbrace{\mathbf{k}_{x_1' x_o} + \mathbf{k}_{g x_o}}^{\mathbf{k}}), \qquad (7)$$

where $\delta M(\mathbf{k}_x,\mathbf{k}_z)$ is the spectrum of the reflectivity model $\delta m(\mathbf{y})$. This equation says that the migration image $\delta m(\mathbf{x})^{\text{mig}}$ is a bandlimited approximation to the actual reflectivity image $\delta m(\mathbf{x})$. The model wavenumbers $\mathbf{k} = \mathbf{k}_{x_1' x_o} + \mathbf{k}_{g x_o}$ are bandlimited partly because the geophone aperture on the surface is finite and there is only one pair of scatterers.

However, equation 6 implies that resonance effectively increases effectively the source frequency from ω to $\omega^{eff} = (2N+1)\omega$, and so increases the model wavenumber from $\omega\nabla\tau_{x_o x_1}$ to $\omega(2N+1)\nabla\tau_{x_o x_1}$. For the Figure 2c example, the horizontal resolution limit for $\mathbf{k}_{x_1 x_o}$ becomes $\Delta x = \pi c/\omega^{eff} = 0.5\lambda/3$ so that far-field superresolution imaging is theoretically possible[3] for $N \geq 1$.

Practical Imaging of Resonance

In practice primaries, not multiples, are migrated to the reflectors of origin so that far-field superresolution is not feasible with standard migration. However, non-linear least squares reverse time migration (RTM) or full wave inversion (FWI) updates the background reflectivity after each iteration. Doing so means that the background wavefields can contain both primaries and multiples, which can build up the natural migration operator for imaging both primaries and multiples to achieve superresolution. Another possibility is to use the Marchenko equations (Wapenaar et al., 2013) to iteratively reconstruct natural Green's functions at depth from surface measurements, which should include strong resonance energy near layers with strong impedance contrasts. These Green's functions can be used to form migration operators that contain the resonant multiples.

Other iterative algorithms have been developed (Soni and Verschuur, 2013) that theoretically predict and invert all internal multiples in the data under ideal circumstances. This work improves upon earlier developments for predicting internal multiples from surface seismic data (Jakubowicz, 1998a-b; ten Kroode, 2002; Ikelle, 2006).

[3] N cannot be too large because each roundtrip returns a weaker signal due to attenuation, geometrical spreading and transmission loss effects.

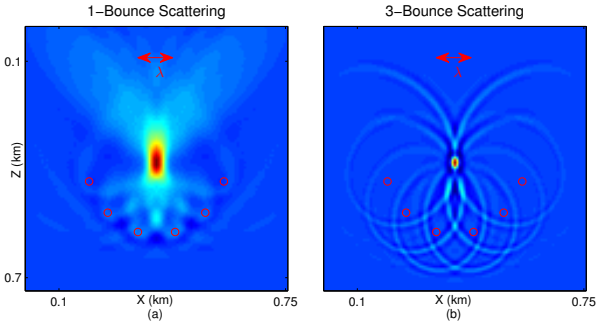

Figure 3: Migration images subject to 6 reference scatterers indicated by ∘, when (a) one bounce takes place between the trial image point and any one of the scatterers, or (b) three bounces take place between the trial image point and each of the 6 scatterers. The bouncing condition is applied consistently in both forward modeling and migration.

NUMERICAL RESULTS

Imaging results for two numerical experiments will be presented. The first one is for shot gathers simulated in the Figure 3 model of an unknown scatterer surrounded by six scatterers with known positions. The resonance is for 3-bounces between the central scatterer and any one of its six neighbors, with rays similar to those in Figure 1b. Figure 3a shows the resulting migration image when only the one bounce data (see Figure 1a) are migrated. Here, a horizontal resolution limit no better than Abbe resolution is obtained. In contrast the three-bounce resonance data are migrated to give the Figure 3b image, where the resolution limit decreases by the expected factor of three. Compared to the wavelength indicated by the two-sided arrow, superresolution imaging is achieved.

The other model is the complicated two-box model in Figure 4a. The associated data will be generated by a finite-difference method and the data inverted by full waveform inversion. Frequencies below 5 Hz are absent from the data as shown in Figure 4b, and the maximum source-receiver offset of 3 km is used for the synthetic data. The shallow rectangular anomalies are larger in size than the minimum effective wave-

DOI http://dx.doi.org/10.1190/segam2014-0344.1

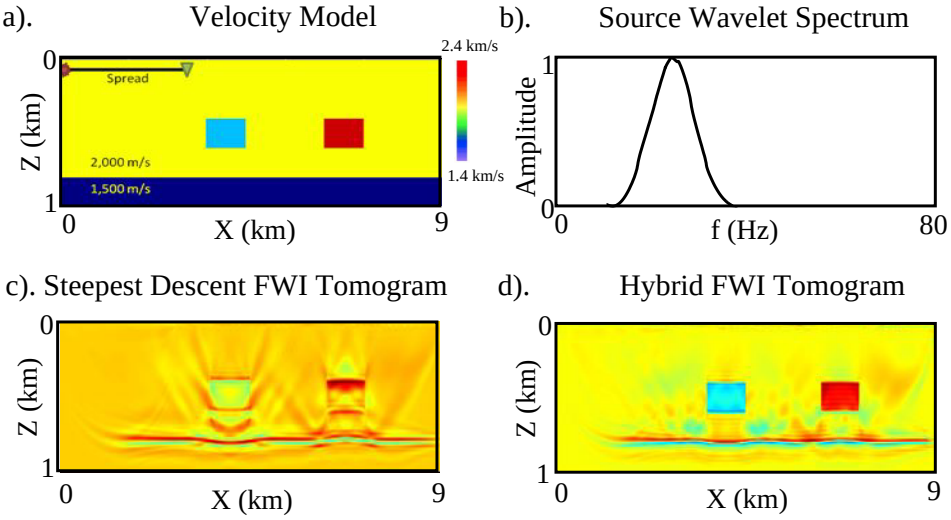

Figure 4: a) Blocky FWI test model, b) Spectrum of the source wavelet used in modeling and inversion, c) Inversion using standard FWI, and d) FWI result with using LSRTM as an internal loop. The initial velocity model for FWI is a homogeneous medium with a constant velocity of 2000 m/s. Images from AlTheyab and Xin (2013).

length associated with the data. The data on the top surface are inverted by a non-linear full waveform inversion (FWI) method that uses least squares migration (LSM) as an inner loop to the full waveform inversion loop (Altheyab and Wang, 2013). The LSM is used to create sharp interfaces along the boundaries so as to develop reflection wavepaths within and outside the boxes. Without the sharp boundaries, standard FWI fails to reconstruct the shallow anomalies as shown in Figure 4c.

As shown in Figure 4d, the Hybrid FWI make use of reflections, diffractions, multiples and prism waves to construct the anomalies and delineate the boundaries with high resolution. The mispositioning of the deeper reflector due to the shallow velocity error is reduced and the reconstructed reflector is nearly flat. In contrast, the reflectors in the standard FWI tomogram in Figure 4c are more distorted because the deeper reflections are not fully utilized for the same number of iterations.

If the highest usable frequency is 40 Hz, then the shortest wavelength is just 50 meters. This is deemed to be insufficient for reconstructing the sharp corners of the box in Figure 4d. However, resonant scattering within and between the boxes, as well as reverberations between the boxes and the deep horizontal layer, are likely contributors to the extremely sharp resolution of the box's corners. It is also possible that scattering around the sharp corners of the box also utilize the high wavenumbers in the evanescent portion of the diffraction wavefields.

CONCLUSIONS

We theoretically and numerically show that superresolution imaging in the far field region of the sources and receivers is theoretically possible if resonant multiples are migrated. For a source with frequency f, N roundtrips in propagating between two scatterers increases the effective frequency to $2N \times f$ and decreases the effective wavelength to $\lambda/2N$.

The most significant challenge in obtaining superresolution is to estimate the background reflectivity accurately enough to achieve superresolution imaging. The numerical results shown in this extended abstract suggest that this might be possible with either non-linear least squares migration or full waveform inversion.

One of the implications of this study is that interbed multiples can, in principle, be used as high-frequency probes to estimate detailed properties of layers. This is not only applicable to crustal reflections or multiple reflections from the top or bottom of salt bodies, but also to mantle and core reverberations studied by earthquake seismologists.

ACKNOWLEDGMENTS

We wish to thank the sponsors of Center for Subsurface Imaging and Fluid Modeling (CSIM) at KAUST for their financial support.

DOI http://dx.doi.org/10.1190/segam2014-0344.1

http://dx.doi.org/10.1190/segam2014-0344.1

EDITED REFERENCES

Note: This reference list is a copy-edited version of the reference list submitted by the author. Reference lists for the 2014 SEG Technical Program Expanded Abstracts have been copy edited so that references provided with the online metadata for each paper will achieve a high degree of linking to cited sources that appear on the Web.

REFERENCES

AlTheyab, A., and X. Wang, 2014, Hybrid linear and non-linear full-waveform inversion of Gulf of Mexico data: 84th Annual International Meeting, SEG, Expanded Abstracts, 1003–1007.

Bleistein, N., 1984, Mathematical methods for wave phenomena: Academic Press.

de Fornel, F., 2001, Evanescent waves: From Newtonian optics to atomic physics: Springer-Verlag.

Fink, M., 2008, Time-reversal waves and super resolution: Journal of Physics: Conference Series, **124**, no. 1, http://dx.doi.org/10.1088/1742-6596/124/1/012004.

Ikelle, L. T., 2006, A construct of internal multiples from surface data only: The concept of virtual seismic events: Geophysical Journal International, **164**, no. 2, 383–393, http://dx.doi.org/10.1111/j.1365-246X.2006.02857.x.

Jakubowicz, H., 1998a, Wave equation prediction and removal of interbed multiples: 60th Conference & Exhibition, EAGE, Extended Abstracts.

Jakubowicz, H., 1998b, Wave equation prediction and removal of interbed multiples: 68th Annual International Meeting, SEG, Expanded Abstracts, 1527–1530.

Lerosey, G., J. de Rosny, A. Tourin, and M. Fink, 2007, Focusing beyond the diffraction limit with far-field time reversal: Science, **315**, no. 5815, 1120–1122, http://dx.doi.org/10.1126/science.1134824.

Schuster, G. T., S. Hanafy, and Y. Huang, 2012, Theory and feasibility tests for a seismic scanning tunnelling macroscope: Geophysical Journal International, **190**, no. 3, 1593–1606, http://dx.doi.org/10.1111/j.1365-246X.2012.05564.x.

Soni, A. K., and D. J. Verschuur, 2014, Full wavefield migration of vertical seismic profiling data: Using all multiples for imaging away from the well: Geophysical Propecting, doi: 10.1111/1365-2478.12130.

ten Kroode, F., 2002, Prediction of internal multiples: Wave Motion, **35**, no. 4, 315–338, http://dx.doi.org/10.1016/S0165-2125(01)00109-3.

Wapenaar, K., F. Broggini, E. Slob, and R. Snieder, 2013, Three-dimensional single-sided Marchenko inverse scattering, data-driven focusing, Green's function retrieval, and their mutual relations: Physical Review Letters, **110**, no. 8, 084301–084305, http://dx.doi.org/10.1103/PhysRevLett.110.084301.